J Mater Sci (2010) 45:1425–1431
DOI 10.1007/s10853-009-3947-0

INTERFACE SCIENCE

Assessment of interface damage during the deformation of carbon nanotube composites

Chih-chuan Kao · Robert J. Young

Received: 3 July 2009 / Accepted: 2 October 2009 / Published online: 23 October 2009

Abstract The deformation micromechanics of single-walled carbon nanotubes in a polymeric matrix was studied through the use of Raman spectroscopy. The variation of stress sensitive G' band positions was used to detect the interfacial adhesion between the nanotubes and the matrix when the composites were subjected to a cyclic deformation process. It was found that the level of the interfacial adhesion decreases with the maximum loading strain and the repeated loading cycles. The debonding phenomenon was saturated by the third cycle of loading of the composites up to 1.0% strain. A hysteresis loop was observed to develop due to the change of the stress transfer efficiency between the loading and the unloading steps when the sample was deformed over 0.4% strain. By analysing the loop area, the energy dissipated in the deformation of the composite materials was investigated and the extent of the interface damage was also assessed.

Introduction

The degree of the interfacial adhesion between the reinforcements and the polymeric matrix is a critical aspect of a composite system. The stress can be transferred effectively from a matrix to reinforcements through an intact interface so that the composites can share the load and sustain higher degree of deformation. Damage and failure of the interface introduces a change of stress transfer such that the mechanical properties of the composite materials may be inferior to those of the matrix. Since carbon nanotubes were discovered more than a decade ago [1–3], they have become an ideal candidates to reinforce polymers due to their exceptional mechanical properties such as a tensile modulus of about 1 TPa [4, 5]. With nanotubes possessing a very high aspect ratio, a large interfacial area is obtained as a stress transfer medium which therefore enhances the reinforcing effect further in the composite system.

The deformation micromechanics of nanotube composites can be determined by utilising microscopic [6–8] or spectroscopic [9, 10] techniques. The level of interfacial adhesion can be measured from the nano pull-out of an individual nanotube embedded in a polymer matrix by using an AFM tip, and the nano-mechanical process can be directly visualised under a microscope. The pull-out energy and other valuable parameters, such as interfacial shear strength, can be measured to assess the degree of interfacial adhesion. The technique is, however, limited to how well the AFM can manipulate the nanotube according to its size. Raman spectroscopy has been proved to be a powerful tool in the nanotube research. As well as the technique being able to characterise the nanotube structure, the nanotube Raman bands are found to shift either in their positions (G and G' band) [10–15] or in their intensities (radial breathing modes) [16–18] with deformation. The stress sensitive Raman bands have been extensively used to monitor the stress transfer behaviour of nanotube composites and to evaluate the degree of interfacial adhesion.

This study aims to evaluate the degree of interfacial adhesion from the stress transfer behaviour of a nanotube composite detected by the variation of the G' band positions subjected to cyclic deformation processes. It is then concerned with the repeated loading of the intact nanotube–matrix interface through several cycles of loading and unloading of the composites. The results have been

C. Kao · R. J. Young (✉)
Materials Science Centre, School of Materials, University of Manchester, Grosvenor Street, Manchester M1 7HS, UK
e-mail: robert.young@manchester.ac.uk

analysed to determine the energy dissipated during the deformation of the composites, as well as the strength of the interface. The approximate extent of the interfacial damaged in the cyclic deformation processes has also been predicted.

Experimental

The nanotube composites were produced using purified HiPco single-walled carbon nanotubes (SWNTs) and a cold-cured epoxy resin system consisting of 50 parts by weight of Araldite LY 5052 epoxy resin and 19 parts by weight of Araldite hardener HY 5052. About 0.1 wt% of the nanotubes, with respect to the total weight of the epoxy resin, were suspended in the hardener and dispersed using sonication and a magnetic stirrer at room temperature for 6 and 2 h, respectively. The epoxy resin was then added into the well-dispersed mixture and degassed in a vacuum chamber before curing the composite at room temperature for 7 days. The use of a cold-cured system led to less residual stress in the material [12].

The nanotube composites produced were cut in to rectangular strips and a strain gauge was attached to the surface of the sample using cyanoacrylate adhesive in order to monitor the level of deformation. The specimen was then inserted into a custom-built four-point bending rig and located on the Raman microscope stage. Two different sets of cyclic deformation tests were included in this study:

- loading and unloading the sample up to an increasing maximum strain level
- loading and unloading the sample up to the same maximum strain level.

For the first experiment, the specimen was gradually loaded up to 0.2, 0.4, 0.6, 0.8 and 1.0% strain, respectively. When the maximum strain was achieved, the sample was released to 0% strain. For the second experiment, a total of five cycles of loading the sample up to 1.0% maximum strain were performed. When the strain reached its maximum value for each loading cycle, the sample was unloaded to 0% strain. It should be noted that the sample used in the first test was from the same batch of material but different from that used in the second test.

The nanotube Raman spectra were collected using a Renishaw 1000 Raman microprobe system with a incident 633 nm He–Ne laser polarised parallel to the tensile axis. A 50× lens was used to focus the laser on the surface of the sample and a spot size of 2 μm was obtained. In both of the cyclic deformation tests, the spectra were collected at intervals of around 0.05% strain and the exciting laser beam was blocked while the deformation process was taking place in order to minimise sample heating. It should be pointed out that all of the spectra were collected from the same area on the sample in each test to detect the in situ deformation behaviour of the composite. The G' spectra were curve-fitted using Lorentizian routines to determine their peak positions.

Results and discussion

The characteristics of the G' band under various deformation states are shown in Fig. 1. The G' band is located at around 2600 cm^{-1} and is well known as an overtone of the D band. It also behaves similarly to the G band but the sensitivity to deformation is much higher than the D and the G bands [10]. It can be seen from the figure that the G' band shifts to lower wavenumber with tension. When the sample was released to 0% strain, the G' band position moved back and slightly towards to higher wavenumber.

Cyclic deformation up to increasing maximum strains

Figure 2 shows the variation of the G' band position in the cyclic deformation range from 0.2 to 0.6% strain. It can be seen that the G' band shifts approximately linearly with strain and the loading curve overlaps the unloading one for the initial two cycles which indicates the stress is fully transferred from the matrix to the nanotubes. The nanotubes can be repeatedly deformed elastically, as well as retaining the interfacial adhesion with the matrix, within this strain range, 0–0.4% strain.

As the maximum loading strain is increased, the strain–shift relationship of the G' band becomes non-linear for the loading cycle, whereas the behaviour remains linear during

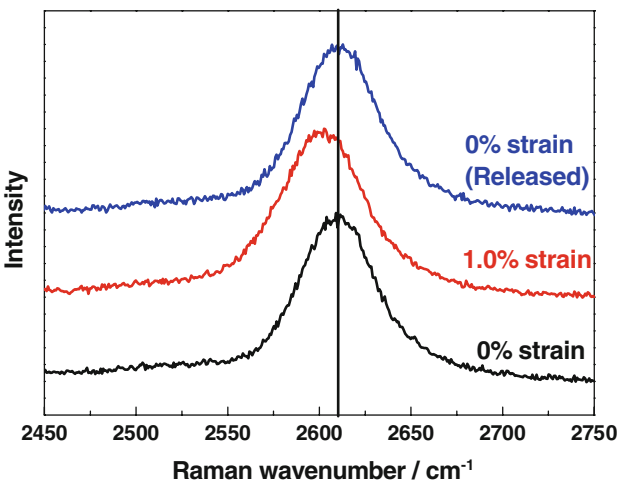

Fig. 1 Shift of the Raman G' band with the strain. The intensity has been normalised and offset for clarity. The *vertical line* indicates the G' peak position centred at around 2610 cm^{-1} for the sample in the undeformed state

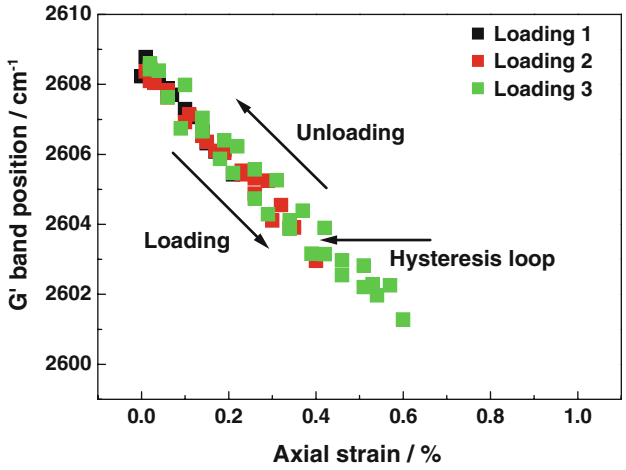

Fig. 2 Shift of the Raman G' band for cyclic deformation for 0.2–0.6% maximum loading strain. The data shown are for both loading and unloading. The occurrence of a hysteresis loop at 0.6% strain as indicated

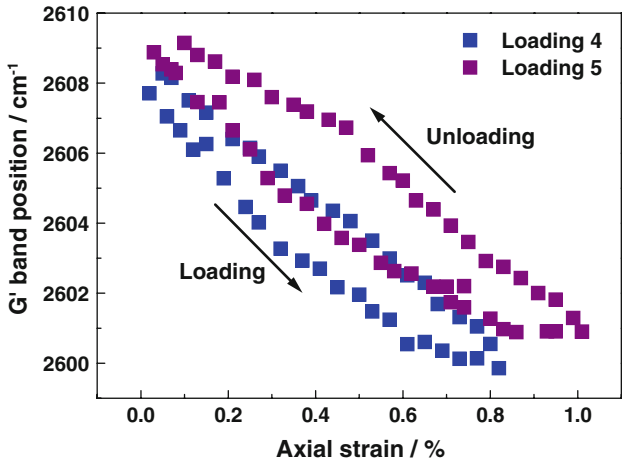

Fig. 3 Shift of the Raman G' band for cyclic deformation for 0.8 and 1.0% maximum loading strain for the same sample used in Fig. 2. The data shown are for both loading and unloading

the unloading cycle. Due to the discrete loading and unloading behaviour, a hysteresis loop is observed for cycles 3, 4 and 5 shown in Figs. 2 and 3 and the loop area is found to increase in size with the level of the maximum loading strain. This behaviour could be due to the composite being subjected to interfacial damage due to the reversible slippage of the nanotube–nanotube layers in the nanotube bundles and/or the permanent damage of the nanotube–matrix interface. Another cyclic deformation study [19] has reported that overlap of the loading and unloading curves is still observed after the nanotube–matrix interface is damaged. As the intensity ratio of the D to the G band was found to remain unchanged in this overlap region, the behaviour was attributed to the slippage taking place within the nanotube–nanotube layers in the bundle during the deformation process. Referring to our observations, it is likely that the hysteresis loop found in this study may be due to the damage at the nanotube–matrix interface. Since the interface was damaged during the loading process, the stress transfer efficiency between matrix and nanotubes changes in the unloading process leading to the observation. In addition, other evidence can be seen in the comparison between the results in cycles 4 and 5. It is clear that the strain–shift profile of the G' band in cycle 5 moves to higher wavenumber compared to the previous cycle. It suggests that the interface is subjected to irreversible damage in the composites and the two loading curves are therefore not followed. The behaviour is similar to cyclic deformation studies on other nanocomposite materials [20].

Loading and unloading to the same maximum strain

Figure 4 shows the mechanical response of nanotubes when the composites were repeatedly deformed up to 1.0% strain. It should be pointed out that only initial three cycles of loading and unloading results are shown here for clarity as cycles 4 and 5 behave similarly and overlap cycle 3. The typical deformation behaviour of nanotube/epoxy composites followed by Raman spectroscopy shows three regions [10, 12, 16]: elastic deformation in the form of linear behaviour observed up to around 0.4% strain, a change in stress transfer in the form of non-linear behaviour from 0.4 to about 0.8% strain and complete interfacial breakdown in the plateau region when the strain is over 0.8%. It is clear that these three regions can only be seen in

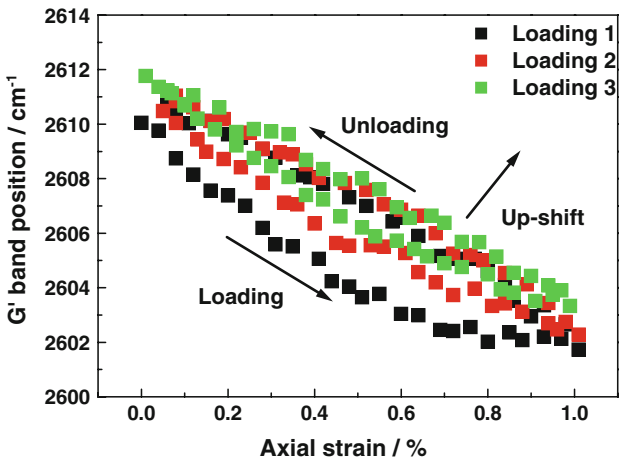

Fig. 4 Shift of the Raman G' band for three cycles of loading and unloading of the sample up to 1.0% maximum strain. The data shown are for both loading and unloading. The profile of the G' band shift with strain moves towards to higher wavenumber and the observed loop area decreases with the number of loading cycles

first loading cycle. Since approximately linear behaviour was obtained in the subsequent cycles, it may suggest that most of interfacial damage occurred during first loading cycle. During the subsequent deformation, the damage continues to develop a little more, since the loading curves become up-shifted in band position with each deformation cycle.

Furthermore, another interesting observation arises from the comparison between the initial band positions for each loading cycle. The zero-strain band position has been found to shift to higher wavenumber in the subsequent loading cycles. It implies that the composite becomes subjected to a residual compressive stress in this cyclic deformation process. We quantified this residual stress by using the universal band shift rate of -5 cm^{-1} GPa [10] for carbon fibres. Residual compressive stresses of about 0.13 GPa were obtained in the first set of tests after the five loading cycles up to an increasing maximum strain and 3.0 GPa in the second set after the five loading cycles up to the same maximum strain of 1%.

Energy dissipation

In the composites

Since a hysteresis loop was observed in our study, it represents the energy dissipated in the composite system during the deformation process. The amount of the energy dissipated per unit volume can be quantified simply by estimating the loop area. The stress–strain curve for a loading and unloading cycle is shown in Fig. 5 to demonstrate the determination of the energy dissipated. It should be noted that the variation of energy estimated is calculated to have an accuracy of within ±10%. The stress value in the figure was derived from the nanotube band shift in G' band wavenumber divided by a universal band shift rate of -5 cm^{-1} GPa for G' band in carbon fibres. The loading and unloading results were curve-fitted using polynomial and linear equations, respectively. However, since linear behaviour was observed in the loading cycles up to 0.2 and 0.4% maximum strain as the data shown in Fig. 2, these loading results were also curve-fitted by using linear functions. The loading and unloading energies were measured by integration of the curve-fitted equations between 0% and the maximum loading strain. Subsequently, the energy dissipated in the deformation cycle was estimated by subtracting the unloading energy from the loading energy. The results in these two cyclic deformation tests are listed in Table 1.

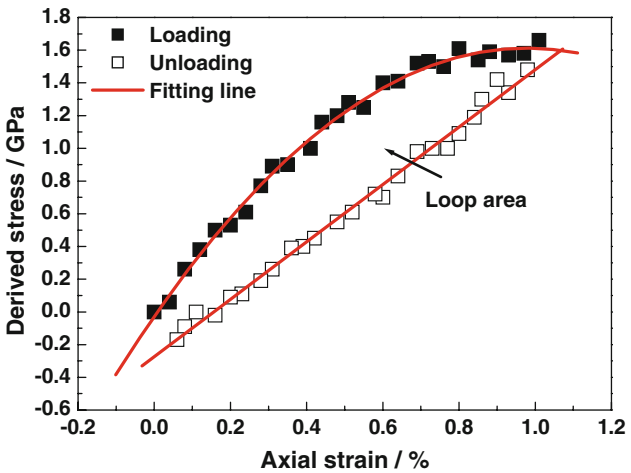

Fig. 5 Derived stress–strain curve of the nanotube composites subjected to a cycle of loading and unloading tests demonstrating the estimation of the loop area. The stress was determined from the universal G' band shift rate, of -5 cm^{-1} GPa, for carbon fibres

Table 1 Energy dissipation in the SWNT/epoxy composites for the two different sets of loading and unloading tests

	Loading energy (MJ m^{-3})	Unloading energy (MJ m^{-3})	Energy dissipated (MJ m^{-3})
Maximum loading strain (%)			
0.2	0.5	0.4	0.1
0.4	2.2	2.0	0.2
0.6	4.9	4.1	0.8
0.8	7.8	5.2	2.6
1.0	10.4	6.7	3.7
Loading cycles (to 1.0% strain)			
Cycle 1	10.8	6.0	4.8
Cycle 2	9.7	6.9	2.8
Cycle 3	10.0	8.1	1.9
Cycle 4	10.2	8.1	2.1
Cycle 5	10.4	8.4	2.2

At the interface

The estimation of the energy dissipated in each cycle and the predication of the level of damage at the nanotube–matrix interface were carried out using the following assumptions. The composites produced in this study were assumed to contain a uniform and randomly oriented nanotube distribution in the polymeric matrix system. The rotation of the nanotubes during the deformation process was neglected in this low strain range ($\leq$1.0% strain). Since the density of the epoxy resin used is about 1.1 g cm^{-3} [21] which is similar to the HiPco SWNT density (of 1.3 g cm^{-3}) [22], the volume fraction of the nanotubes (V_f) is about 0.1% for approximately 0.1% by weight of nanotubes dispersed in the epoxy resin. The volume (V_{nt}) of the nanotube can be calculated from their length (L) and diameter (D) and the number of nanotubes

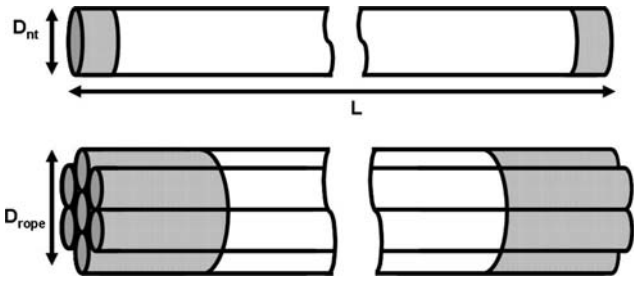

Fig. 6 Schematic diagram of an individual nanotube and a nanotube bundle. *D* and *L* represent the diameter and the length of the nanotube and the *grey area* indicates the interface damage area accumulated from the cycles of loading and unloading

(N) per unit volume of the polymeric matrix can be estimated though the following equation:

$$V_{nt} = (D/2)^2 \pi L = (D^2 \pi L)/4$$
$$N = V_f / V_{nt} = \frac{4V_f}{D^2 \pi L} \quad (1)$$

It should be pointed out that D can be either the diameter of an individual nanotube (D_{nt}) or the diameter of a nanotube bundle or rope (D_{rope}), as the diagram in Fig. 6 shows, depending on the degree of dispersion of the nanotubes in the matrix. In this case, the total area of the nanotube–matrix interface (A'_{nt}) per unit volume of the composites can be assessed from the nanotube surface area (A_{nt}) attached to matrix multiplied by the number of nanotubes in per unit volume of composites as follows:

$$A_{nt} = D\pi L$$
$$A'_{nt} = A_{nt} \times N = D\pi L \times \frac{4V_f}{D^2 \pi L} = \frac{4V_f}{D} \quad (2)$$

The unmodified epoxy resin was also tested in tension in our study (data not shown). The stress–strain curve was linear up to well over 1% strain, which suggests that the epoxy resin would be expected to undergo the elastic deformation within the maximum 1.0% loading strain used in this study. The loop generated in the cyclic deformation process must therefore be attributed mainly to nanotube–matrix interfacial debonding. The energy dissipated at the interface ($E_{Interface}$) can then be determined from the energy dissipated in the composite (E_{comp}) divided by total nanotube–matrix interface area:

$$E_{Interface} = \frac{E_{comp}\ (\mathrm{MJ\ m^{-3}})}{A'_{nt}\ (\mathrm{m^2\ m^{-3}})} \quad (3)$$

Substituting Eq. 2 into Eq. 3 gives,

$$E_{Interface} = \frac{DE_{comp}}{4V_f}\ (\mathrm{J\ m^{-2}}) \quad (4)$$

It is clear that the energy dissipated at the interface is very dependent on the nanotube diameter and the volume fraction of the nanotubes in the polymer. The results shown in Figs. 7 and 8 for two different cyclic deformation tests were evaluated from the assumption of the composite containing individual nanotubes with an average diameter of 1 nm.

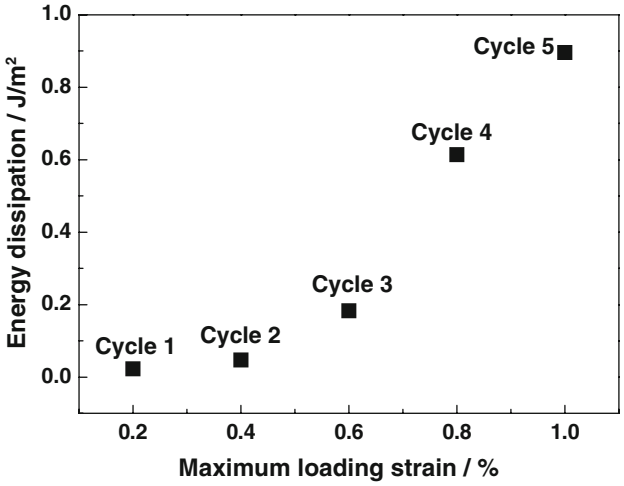

Fig. 7 Interfacial energy dissipated during the cyclic deformation up to different maximum loading strains. The amount of the energy dissipated was estimated from assuming 0.1 wt% of nanotubes dispersed in the matrix system with dimensions of 1 nm in diameter and 1 μm length

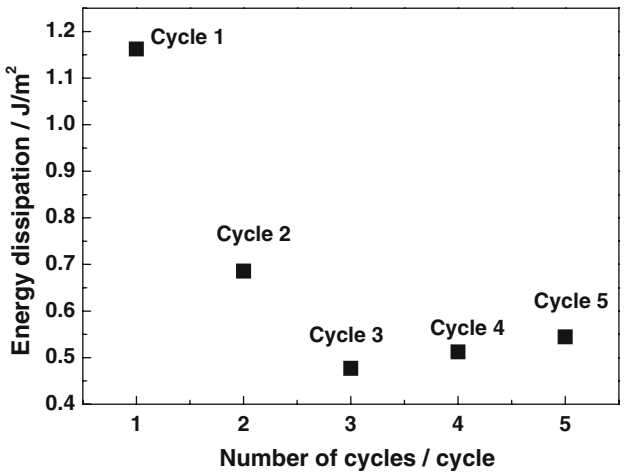

Fig. 8 Interfacial energy dissipated during the cyclic deformation up to 1% maximum loading strain. The amount of the energy dissipated was estimated from assuming 0.1 wt% of nanotubes dispersed in the matrix system with dimensions of 1 nm in diameter and 1 μm length

It can be seen from Fig. 7 that no significant energy dissipation was found at 0.2–0.4% maximum loading strains due to the good bonding between nanotubes and matrix. As the maximum strain increased, a steep build-up in the energy dissipation was observed, indicating the steady development of interfacial breakdown.

The results in Fig. 8, however, show that a great deal of energy dissipation occurred for the initial two loading

cycles and that it tends to be constant over the subsequent loading cycles. As mentioned previously, the G' band strain–shift profiles were overlapped among cycles 3, 4 and 5, which may imply the termination of the development of further interface damage. This could be due to two possible reasons: the interface might have failed completely in the earlier cycles or the applied strain level may not be high enough to cause any further damage of the interface. Therefore, under these circumstances, the approximately constant energy dissipation observed may be due to friction at the damaged nanotube–matrix interface during the deformation process.

The degree of the adhesion of individual nanotubes in a matrix has been determined using a nano "pull-out" test [6]. In particular, the energy required to damage the nanotube–polymer interface ($E'_{\text{Interface}}$) can be measured from this nanomechanical test. In this case, the extent of the damaged interface (L_{D}) can be estimated approximately from a comparison between the pull-out energy and the interface dissipation energy observed in our study:

$$L_{\text{D}} = \frac{E_{\text{Interface}}}{E'_{\text{Interface}}} \times 100\% = \frac{DE_{\text{comp}}}{4V_{\text{f}}E'_{\text{Interface}}}(\%) \quad (5)$$

Cooper et al. [6] pulled out individual SWNTs bridged across a hole of an epoxy resin and reported that an energy ($E'_{\text{Interface}}$) of the order of 25 J m^{-2} was required to break the SWNT–epoxy interface completely. The extent of interface damage in our study can be evaluated from their findings. The results listed in Table 2 were estimated for different nanotube dispersion morphologies in the composite system ranging from individual nanotubes (1 nm diameter, factor 1), nanotube bundles (factor 7; the closed-packed geometry is shown in Fig. 6) and nanotube assemblies (factor 49; an assembly of seven bundles). The extent of interface damage determined for the two different sets of loading and unloading experiments (estimated using factors 1 and 49) is shown in Figs. 9 and 10.

Since an overlap of the loading and unloading curves was found in the low strain deformation region, a near-zero damaged interface shown in Fig. 9 is as expected. At higher maximum loading strains, a damaged interface develops from the both ends of the nanotube (Fig. 6) and results in the increase in energy dissipation. Moreover, Fig. 10 shows a less damaged interface with increasing loading cycles. If the constant energy dissipation for cycles 3, 4 and 5 was due to the friction taking place at the damaged interface, it implies that the amount of the energy dissipation obtained at cycles 1 and 2 is not only attributed to the interfacial breakdown, but also to the friction at the

Table 2 Extent of damage interface for the two different sets of loading and unloading tests

	Factor 1 (isolated NT) (%)	Factor 7 (NT bundles) (%)	Factor 49 (NT bundles) (%)
Maximum loading strain (%)			
0.2	0.09	0.27	1.06
0.4	0.18	0.55	2.14
0.6	0.71	2.15	8.30
0.8	2.40	7.19	27.80
1.0	3.50	10.50	40.58
Loading cycles			
Cycle 1	4.54	13.62	52.67
Cycle 2	2.68	8.04	31.08
Cycle 3	1.86	5.59	21.62
Cycle 4	2.00	6.00	23.21
Cycle 5	2.13	6.39	24.69

The results presented were estimated assuming various nanotube dispersion morphologies in matrix system

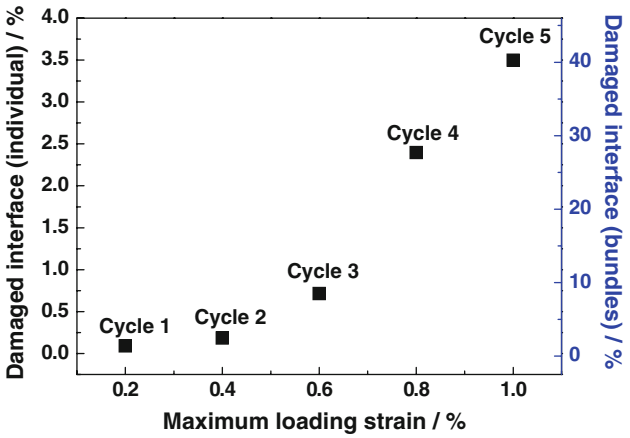

Fig. 9 Extent of the interface damage predicted for either the individual nanotubes or the nanotube bundles in the matrix for the cyclic deformation up to different maximum loading strains

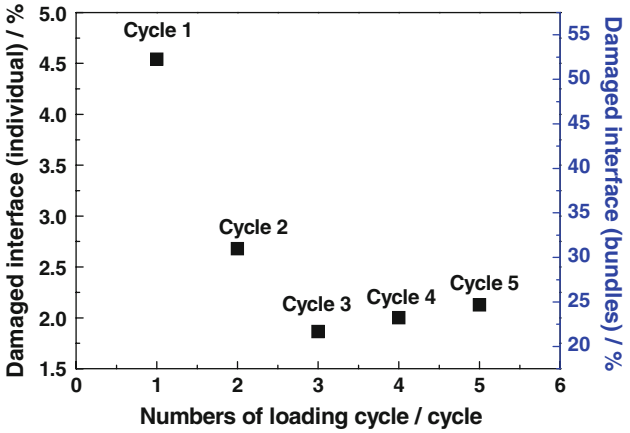

Fig. 10 Extent of the interface damage predicted for either the individual nanotubes or the nanotube bundles in the matrix for the cyclic deformation up 1% maximum loading strain

damaged interface. Therefore, the extent of the interface damaged determined is probably an upper limit and actually much less than the values presented in Figs. 9 and 10.

The level of interface damage estimated varies according to the dispersion morphologies of the nanotubes in the matrix system. It can be seen from Eq. 5 that the extent of the interface damage depends directly on the nanotube diameter which is related to the dispersion in the composites. If the dispersed morphology is the close-packed nanotube bundle assembly (Fig. 6) for which the diameter (D_{rope}) is much larger than an individual nanotube (D_{nt}), the number of nanotubes (N) dispersed in per unit volume of the composites is much less. Therefore, a lower nanotube–epoxy interface area (A'_{nt}) is available to accommodate the applied stress. This implies that each nanotube bundle suffers a higher deformation compared to the individual nanotube leading to a higher level of interface damage with bundles.

Conclusions

The study has demonstrated an approach to assess interfacial adhesion in nanotube/epoxy composites through the use of Raman spectroscopy. The degree of the interfacial adhesion was evaluated for cyclic deformation processes and it was found to be dependent on the maximum loading strain and the numbers of deformation cycles. A hysteresis loop was observed from the mismatch between the loading and unloading results and the loop area was estimated in order to evaluate the energy dissipated in the composites. This was employed for further modelling of the approximate extent of the interface damage by making appropriate assumptions about the nanotube distribution in the composite. This approach could also be applied to other types of nanocomposites such as functionalised nanotubes [23, 24] dispersed in various polymeric matrices.

References

1. Iijima S (1991) Nature 354:56
2. Bethune DS, Kiang CH, de Vries MS, Gorman G, Savoy R, Vazquez J, Beyers R (1993) Nature 363:605
3. Iijima S, Ichlhashi T (1993) Nature 363:603
4. Krishnan A, Dujardin E, Ebbesen TW, Yianilos PN, Treacy MMJ (1998) Phys Rev B 58:14013
5. Yu MF, Files BS, Arepalli S, Ruoff RS (2000) Phys Rev Lett 84:5552
6. Cooper CA, Cohen SR, Barber AH, Wagner HD (2002) Appl Phys Lett 81:3873
7. Barber AH, Cohen SR, Wagner HD (2003) Appl Phys Lett 82:4140
8. Barber AH, Cohen SR, Kenig S, Wagner HD (2004) Compos Sci Technol 64:2283
9. Frogley MD, Ravich D, Wagner HD (2003) Compos Sci Technol 63:1647
10. Cooper CA, Young RJ, Halsall M (2001) Composites Part A 32:401
11. Frogley MD, Zhao Q, Wagner HD (2002) Phys Rev B 65:113413
12. Kao CC, Young RJ (2004) Compos Sci Technol 64:2291
13. Kannan P, Young RJ (2007) Nanotechnology 18:235707
14. Hadiev VG, IIiev MN, Arepalli S, Nikolaev P, Files BS (2001) Appl Phys Lett 78:3139
15. Cui S, Kinloch IA, Young RJ, Noé L, Monthioux M (2009) Adv Mater 21:1
16. Lucas M, Young RJ (2004) Phys Rev B 69:08540
17. Cronin SB, Swan AK, Ünlü MS, Goldberg BB, Dresselhaus MS, Tinkham M (2005) Phys Rev B 72:035425
18. Lee SW, Jeong GH, Campbell EEB (2007) Nano Lett 7:2590
19. Kumar R, Cronin SB (2007) Phys Rev B 75:115421
20. Rusli R, Eichhorn SJ (2008) Appl Phys Lett 93:033111
21. Manufacturer's datasheet, Huntsman, UK
22. Zhou X, Shin E, Wang KW, Bakis CE (2004) Compos Sci Technol 64:2425
23. Larsen R (2009) J Mater Sci 44:799. doi:10.1007/s10853-008-3155-3
24. Li SQ, Wang F, Wang Y, Wang JW, Ma J, Xiao J (2008) J Mater Sci 43:2653. doi:10.1007/s10853-008-2489-1